



This is a repository copy of *Steel-Reinforced Grout (SRG) strengthening of shear-critical RC beams*.

White Rose Research Online URL for this paper:
<http://eprints.whiterose.ac.uk/148050/>

Version: Accepted Version

Article:

Thermou, G.E., Papanikolaou, V.K., Lioupis, C. et al. (1 more author) (2019)
Steel-Reinforced Grout (SRG) strengthening of shear-critical RC beams. *Construction and Building Materials*, 216. pp. 68-83. ISSN 0950-0618

<https://doi.org/10.1016/j.conbuildmat.2019.04.259>

Article available under the terms of the CC-BY-NC-ND licence
(<https://creativecommons.org/licenses/by-nc-nd/4.0/>).

Reuse

This article is distributed under the terms of the Creative Commons Attribution-NonCommercial-NoDerivs (CC BY-NC-ND) licence. This licence only allows you to download this work and share it with others as long as you credit the authors, but you can't change the article in any way or use it commercially. More information and the full terms of the licence here: <https://creativecommons.org/licenses/>

Takedown

If you consider content in White Rose Research Online to be in breach of UK law, please notify us by emailing eprints@whiterose.ac.uk including the URL of the record and the reason for the withdrawal request.



eprints@whiterose.ac.uk
<https://eprints.whiterose.ac.uk/>

Steel-Reinforced Grout (SRG) Strengthening of Shear-Critical RC Beams

G.E Thermou^{1*}, V.K. Papanikolaou², C. Lioupis³ and I. Hajirasouliha⁴

¹ Assistant Professor in Structural Engineering, Dept. of Civil Engineering, The University of Nottingham, NG7 2RD, Nottingham, UK

² Assistant Professor, Aristotle University of Thessaloniki, Dept. of Civil Engineering, 54124, Thessaloniki, Greece

³ Civil Engineer, 41335, Larisa, Greece

⁴ Senior Lecturer, Civil and Structural Engineering Department, The University of Sheffield, S1 3JD, Sheffield, UK

Abstract: This paper investigates the effectiveness of Steel-Reinforced Grout (SRG) jackets to strengthen shear critical reinforced concrete (RC) beams. Eleven RC beams were tested in three-point bending. Key parameters of investigation were the strengthening configuration (U- and fully-wrapped jackets), the density of the fabric (1.57 and 4.72 cords/cm) and the number of the strengthening layers (one and two). The test results demonstrated the efficiency of SRG jacketing in increasing both strength (up to 160%) and deformation capacity (up to 450%) of the shear critical beams. Expressions are proposed for estimating the effective strain of the SRG jacket.

Keywords: SRG; FRCM; Jackets; Steel fabric; Mortar; RC Beams; Shear; Strengthening

* Corresponding author, tel: +44 (0) 115 7487229, georgia.thermou@nottingham.ac.uk

1. Introduction

The vast majority of reinforced concrete (RC) structures was built at times when general understanding about the importance of reinforcement detailing in seismic response was still at a premature stage. Poor material and construction quality as well as aging of materials (e.g. steel corrosion) are other key factors that increase the vulnerability of substandard structures to future earthquake events. In the pre-1970s construction practice, shear reinforcement generally comprised of smooth rectangular stirrups anchored with 90° hooks in the ends, made of StI (yield strength 220 MPa) 6–8 mm diameter bars spaced at 250–300 mm on centres along the lengths of beams and columns [1]. Strength hierarchy checks performed on structural members with the aforementioned detailing, revealed that in most cases, and especially for beams, shear failure was the dominant mode of failure [1-3]. Such brittle failures can spread out across different locations of the building and jeopardize the overall structural integrity and ultimately lead to collapses.

In general, using externally bonded composites provides an effective way to alleviate deficiencies at local (member) level associated with shear critical members. Fibre Reinforced Polymer (FRP) jacketing is a popular and effective intervention method that has been used extensively for strengthening of substandard RC structures worldwide [e.g. 4-7]. However, FRP jacketing systems have several drawbacks, mainly related to the use of epoxy, such as poor behaviour to fire conditions, relatively high cost of epoxy resins and lack of vapour permeability with adverse effects on RC structures. In the last few years a new generation of mortar-based systems has been introduced, which retains the advantages of FRP applications but eliminates the previous shortcomings by using mortar instead of resin. Depending on the type of the textile, the following Fibre-Reinforced Cementitious Mortar (FRCM) systems have been developed: (i) TRM (Textile-Reinforced Mortar) where bidirectional textiles made of continuous carbon

or glass fibres are applied using mortars [e.g. 8-10]; (ii) PBO-FRCM (poliparafenilen benzobisoxazole fibre-reinforced cementitious matrix) where PBO nets are embedded in a cement based matrix [e.g. 11-12]; and (iii) SRG (steel-reinforced grout) system where Ultra High Tensile Strength Steel (UHTSS) textiles are combined with inorganic binders [e.g. 13-23].

Several experimental studies have demonstrated the efficiency of TRM and PBO-FRCM jacketing at improving the response of shear critical beams (TRM [24-32], PBO-FRCM [33-37]). Regardless of the adopted textile architecture, the number of layers and the jacket configuration, FRCM jackets have been proved quite efficient in increasing the shear capacity of deficient beams and in some cases activating flexural yielding. In case of SRG jacketing, the research conducted on shear strengthening of deficient RC beams is rather limited. In a recent study, Gonzalez-Libreros et al. [38] tested four beams retrofitted by adding U-shaped SRG jackets made of galvanized unidirectional sheets of an equivalent thickness of 0.27 mm. Parameters of investigation were the shear reinforcement of the beams (2 beams with $\varnothing 6/200$ and 2 beams with $\varnothing 6/300$) and the textile installation (with and without anchors). The SRG jacketed beams failed in shear and similar cracking patterns were observed between the beams with and without anchors. In general, the addition of SRG jackets increased the shear strength of the beams. The presence of the anchors prevented detachment of the composite, but it did not increase the shear strength any further.

The main objective of this paper is to further investigate the role of key design parameters on the response of shear critical beams retrofitted with SRG jackets. An experimental study is carried out where one- or two-layered U-wrapped, U-wrapped with mechanical anchorage and fully-wrapped SRG jackets are applied to nine two-span beams (two additional beams are used as control specimens). The efficiency of two densities of Ultra-High Tensile Strength Steel (UHTSS) textiles is also examined (1.57 and 4.72 cords/cm). The test results demonstrate the effectiveness of SRG jacketing in increasing both strength and deformation capacity of the

shear critical beams. It is shown that the fully-wrapped SRG jackets can substantially modify the response of the original member by allowing it to fail in flexure. The experimental values of the shear strength of the SRG strengthened beams are then compared to the predicted values using existing design guidelines. Based on the experimental data, new expressions are derived which relate the effective strain of the SRG jacket to its axial rigidity.

2. Experimental program

2.1 Specimen Details

Eleven RC beams were tested in three-point bending with a clear span to depth ratio of $a/d = 2.2$. The beams are characterized as short and it is expected that a major portion of the load capacity after the inclined cracking will be due to load transfer by the compression strut. All beams had a rectangular cross section 200 mm in width and 300 mm in height and were 2000 mm long. The beams were divided into two groups (A and B) according to the arrangement of the longitudinal steel reinforcement. Group A comprised one control and four SRG strengthened beams, whereas Group B consisted of one control and five SRG strengthened beams.

The longitudinal tensile and compressive reinforcement in Group A beams comprised two bottom and two top 12-mm diameter bars ($\rho_l = 0.75\%$), respectively (see Fig. 1). In case of Group B, the reinforcement of the beams consisted of longitudinal deformed steel bars with 2 \varnothing 10 bars at the top and 4 \varnothing 16 bars at the bottom of the cross-section of the beam ($\rho_l = 1.60\%$). Deformed steel 8 mm diameter closed stirrups were distributed at a uniform spacing of 100 mm in the longer span 1100 mm in length. All the beams were designed to be deficient in shear in the shorter shear span (600 mm in length, Fig. 1). Although, the presence of transversal internal steel (i.e. stirrups) would influence the response of the SRG jacketed beams, it was decided not to be considered as an additional parameter of study, since the objective was to directly assess

the efficiency of SRG jacketed on the retrofitted beams. Hence, no transverse reinforcement was provided in the critical shorter shear span of 600 mm (Fig. 1), and the SRG jacketing was only applied in the critical shear span. The anchorage zones for the longitudinal reinforcement were 150-mm in length and two stirrups of 8-mm diameter were provided (Fig. 1).

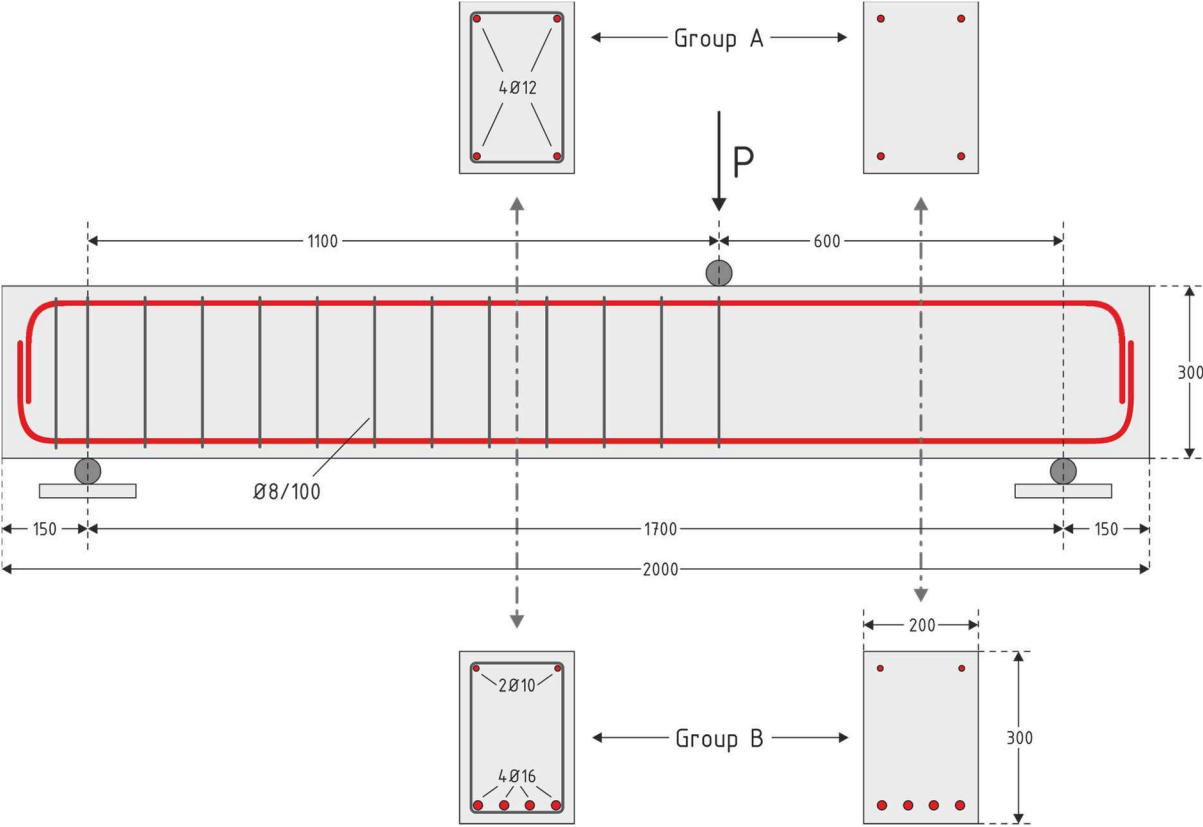


Figure 1: Geometry and reinforcement details of Group A and Group B beam specimens.

The key parameters of investigation were: (i) the density of the Ultra-High Tensile Strength Steel (UHTSS) textile which was 1.57 and 4.72 cords/cm, (ii) the number of applied SRG layers (one and two) and (iii) the strengthening configuration which consisted of U-wrapped, U-wrapped with mechanical anchorage and fully-wrapped SRG jackets. The beams were given the notation XYZW, where X stands for the group of the beams (A or B in Table 1), Y corresponds to the type of the jacketing system with 0 for the control specimen, U for the U-wrapped jacket, UM for the U-wrapped jackets with mechanical anchorage and F for the fully-

wrapped jackets, Z indicates the density of the fabric with L and H for the 1.57 and 4.72 cords/cm fabrics, respectively, and finally W refers to the number of layers with 1 and 2 for single- and double-layered SRG jackets. The details of all test specimens are given in Table 1.

Table 1: Details of the specimens

Group	Name	f_c (MPa)	Type of jacket	Density (cords/cm)	Layers
Group A	A0	28.0	control	-	-
	AUH1		U-wrapped	4.72	1
	AUML1		U-wrapped mechanical anchorage	1.57	1
	AFL1		Fully-wrapped	1.57	1
	AFH1		Fully-wrapped	4.72	1
Group B	B0	23.3	control	-	-
	BUL1		U-wrapped	1.57	1
	BUL2		U-wrapped	1.57	2
	BUML1		U-wrapped mechanical anchorage	1.57	1
	BFL1		Fully-wrapped	1.57	1
	BFL2		Fully-wrapped	1.57	2

2.2 Material Properties

The RC beams of Group A were casted in one batch having an average compressive strength of $f_c = 28$ MPa (standard deviation, SD = 2.47 MPa) at the day of the test obtained from six standard cylinders (150×300mm). The beam specimens of Group B were casted in two batches of three using the same mix. The average compressive strength at the day of the tests was $f_c = 23.3$ MPa (standard deviation, SD = 1.36 MPa), which was determined from the average of six standard cylinders (150 ×300mm). The steel grade used for internal longitudinal (i.e. Ø10, Ø12, Ø16) and transverse reinforcement (i.e. Ø8) was B500C.

In this study, nine beams (four from Group A and five from Group B, see Table 1) were retrofitted by using the SRG jacketing, in which externally bonded Ultra High Tensile Strength Steel (UHTSS) textiles were embedded in an inorganic mortar matrix [13-14]. The textiles were made of galvanized unidirectional high strength steel 3X2 cords fixed to a fiberglass micromesh

to facilitate installation (see Fig. 2). The fiberglass micromesh keeps the cords in place without contributing to strength of the composite system [39, 40]. Each cord was made by twisting five individual wires; three straight filaments wrapped by two filaments at a high twist angle as shown in Fig. 2. The geometrical and mechanical properties of the single cords are given in Table 2 as provided by the manufacturers. More details regarding the stress-strain curve of the cords can be found in Napoli et al. [39] and Santis et al. [40].

Table 2: Geometrical and mechanical properties of single cords as provided by the manufacturer

Cord type	Cord diameter (mm)	Cord area (mm ²)	Break load (N)	Tensile strength f_{fu} (MPa)	Strain to failure ϵ_{fu} (mm/mm)	Elastic modulus E_f (MPa)
3X2	0.827	0.538	1506	2800	0.015	190000

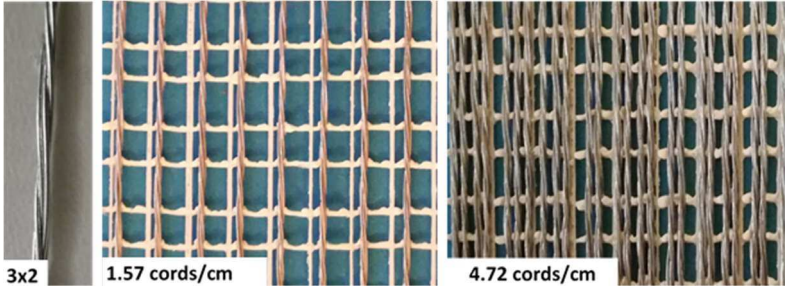


Figure 2: Steel cords and densities of the UHTSS textiles used

One of the critical design parameters of the SRG jacketing technique is the density of the textiles (i.e. the spacing between successive cords) since it should be designed to provide uninhibited flow of the cementitious grout through the steel fabric and develop adequate bond between the textile and the matrix [13]. Two different densities 1.57 and 4.72 cords/cm were examined in this experimental study with an equivalent thickness per unit width for a single layer of steel fabric, t_f , equal to 0.084 and 0.254 mm, respectively (Table 1, Fig. 2). The axial stiffness of the textile, $K_f (= A_f \cdot E_f)$, which is directly related to the density of the textile, was calculated equal to 15960 and 48260 N/mm for the 1.57 and the 4.72 cords/cm textiles, respectively (these figures should be doubled for the two-layered jackets).

A commercial geo-mortar with a crystalline reaction geobinder base and a very low petrochemical polymer content and free from organic fibres was used in this study. The component mortar was utilised as the substrate material applied to the concrete surface of the specimens, the bonding material between the applied layers of the steel fabric and as a final cover. The mechanical properties of the mortar appear in Table 3.

Table 3: Mechanical properties of the mortar at 28 days as provided by the manufacturer

Mortar	Modulus of elasticity E_m (MPa)	Flexural strength f_{mf} (MPa)	Compressive strength f_{mc} (MPa)	Adhesive bond f_{mb} (MPa)
	25000	10.0	55.0	2.0

2.3 SRG Strengthening

As mentioned above, nine RC beams (four from Group A and five from Group B) were strengthened in the 600 mm shear critical span by applying the following three strengthening configurations: U-wrapped, U-wrapped with mechanical anchorage and fully-wrapped SRG jackets (see Table 1). The textiles originally were in roles of 300 mm width, thus 2 and 4 pieces of fabric were utilized for the single- and double-layered SRG jackets, respectively. Before starting the strengthening procedure, the fabrics were cut and pre-bent in order to follow the shape of the jacket (Fig. 3). The edges of the beam cross section were not rounded, hence at these areas the fabrics were pre-bent at right angle. The sides of the beams were roughened using mechanical grinding to expose the aggregates and then were cleaned and saturated with water before proceeding to the application of the mortar (Fig. 4a). Subsequently, the mortar was applied in approximately 3 mm-thick layers manually with the help of a trowel directly onto the lateral surface of the specimens (Fig. 4b). The textile was placed immediately after the application of the cementitious mortar (Fig. 4c) and the mortar was squeezed out between the steel fibres by applying pressure manually. In case of the fully-wrapped one- and two-layered SRG jackets, after the application of the fabric to one and two full-cycles, respectively, the remaining length, which was equal to the width of the beam (200 mm), was lapped over the top

surface of the beam. It should be noted that in the case of two-layered fully-wrapped jackets the fabric was continuous, while in the case of two-layered U-wrapped jacket each layer was independent. Straight after the application of the first layer of the textile, the next layer of the mortar covered it completely and the second layer of the fabric was applied by following the procedure described above. A final coat of the cementitious mortar was applied to the exposed surface. The effect of SRG jacketing on the geometric dimensions of the specimens was small. Each layer of the mortar including the textile was 7 and 10 mm thick for the one- and two-layered SRG jackets, respectively.



Figure 3: Preparation of the UHTSS textiles

In two of the beams (AUML1 and BUML1, see Table 1) a custom-made mechanical anchorage system was applied to enhance the anchorage of the U-wrapped SRG jackets to the concrete substrate. The system comprised four 700×50×5 mm metal plates (2 placed on each side of the beam), which covered the full-length of the strengthened area. The metal plates were drilled at their mid-height so that in total 9 holes were opened with 70 mm spacing (Fig. 5). The beams were drilled following the same pattern and the metal plates attached 50 mm above the upper fibre. Subsequently, the stud anchors were installed and properly wedged in the beam holes. A thin layer of mortar was applied onto the roughened concrete substrate and the fabric was then passed through the anchors and well stretched before the first metal plate was put in place. The free end-zone of the fabric, which was pre-bent, was wrapped over the first metal plate and then the second metal plate was put in place. The last stage involved screwing in the metal plates on each side of the beam to ensure that any sliding of the fabric would be avoided.

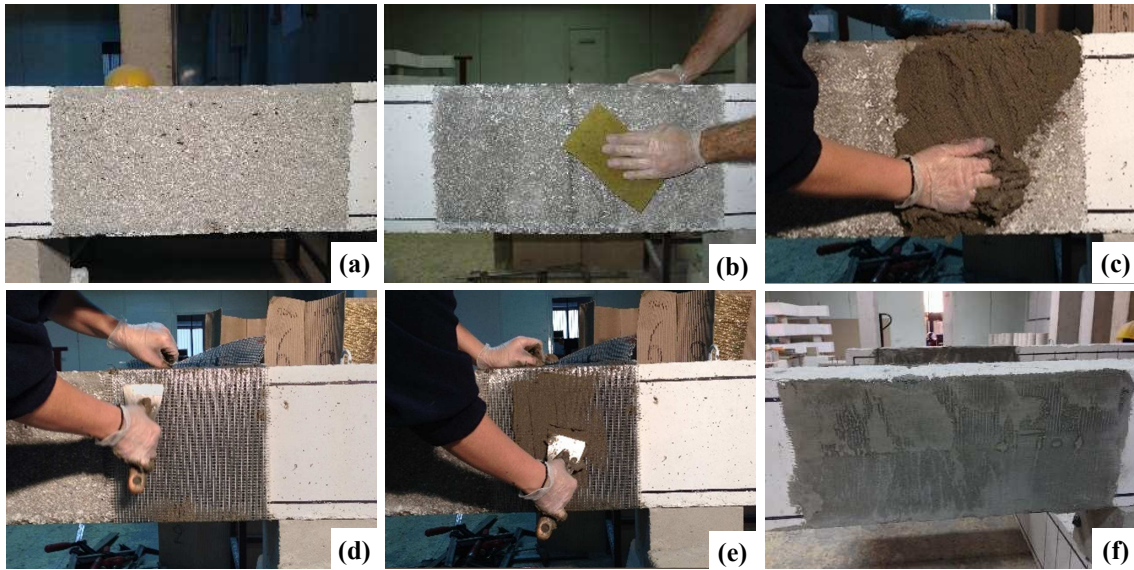


Figure 4: SRG jacketing application steps

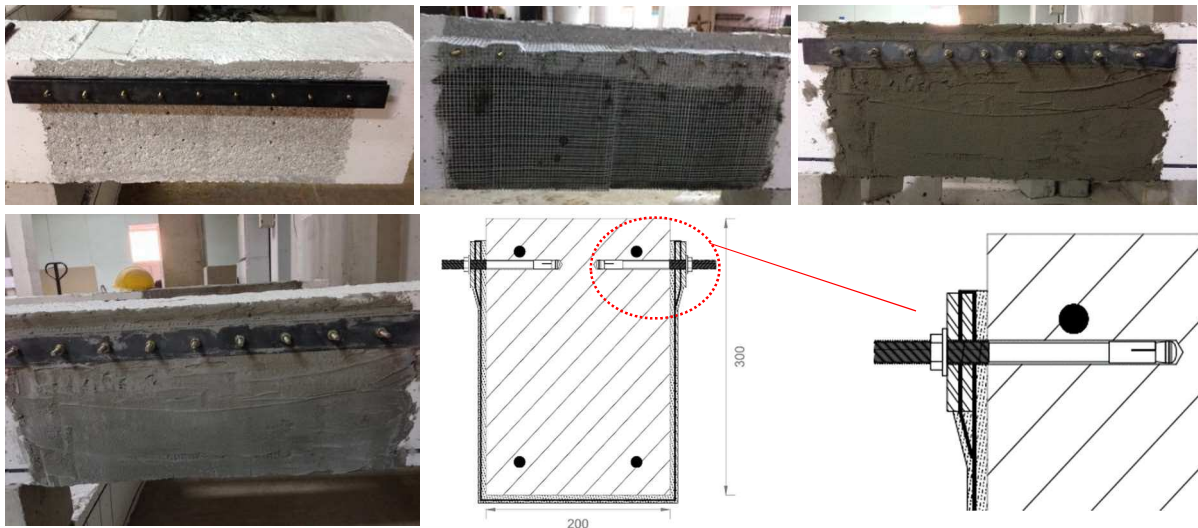


Figure 5: Preparation of the mechanical anchorage of the SRG U-wrapped beams

2.4 Test setup and experimental methodology

The employed three-point bending setup is depicted in Fig. 6. The RC beam was simply supported on a pair of steel pedestals seated on the strong floor and anchored together with a pair of threaded rods in order to prevent transverse sliding (span elongation) due to the second order horizontal reactions at the beam supports. Loading was vertically applied by a 1000 kN capacity single-ended actuator (MTS 243.60) using a displacement control system externally measured by a draw-wire sensor placed underneath the beam along the vertical loading axis.

The external load was monotonically increased up to beam failure, which was triggered upon a 40 % drop of the maximum measured reaction of the actuator load cell. The load was applied at displacement rate 0.05mm/sec. Moreover, a Digital Image Correlation (DIC) configuration was utilised for capturing the strain contours of the tested beams [41]. The shear critical region of each beam (the area of interest (AOI)) was painted with a speckle pattern using a special brush and black ink. A DSLR camera was placed on a tripod at a distance, focusing on the beam's AOI, remotely and automatically shuttered from the main acquisition controller at given displacement intervals (4 photos per mm). Finally, the captured high-resolution speckle images for each specimen were post-processed using a DIC software to produce strain contours at characteristic points on the resulting load-displacement response curve.



Figure 6: Test setup and details of instrumentation

3. Test results and discussion

3.1 Failure modes

The control beams of both Groups A and B (i.e. A0 and B0) exhibited a diagonal tension failure mode as observed in Fig. 7. A single inclined crack along the loading and the support points appeared in the shear span at the early stages of loading, which progressed further as the loading increased leading to a brittle shear failure.

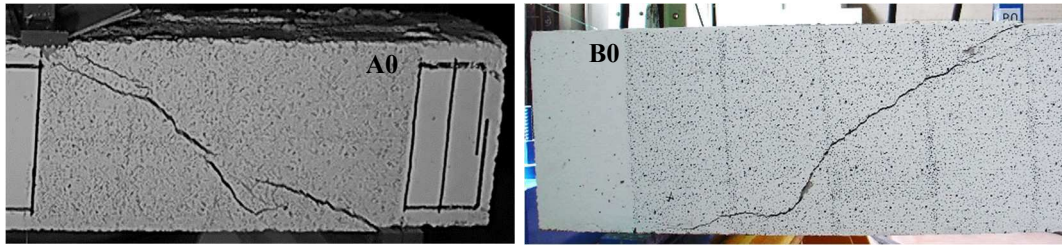


Figure 7: Failure mode of the control specimens

The different SRG jacketing schemes applied to the shear-critical beams of Group A led to flexural failure of the strengthened beams (Fig. 8). The internal bottom steel reinforcement reached yielding and the beams failed in a ductile manner, while flexural cracks formed on both sides of the applied point load (Fig. 8). Apart from the cracks developed along the beam transverse direction that coincided with the gap between successive cords, the textile did not show any further damage.



Figure 8: Failure modes of the SRG-strengthened specimens of Group A

The U-wrapped SRG strengthened beams of Group B (BUL1 and BLU2, Table 1) both failed in shear (Fig. 9). The general mode of failure observed was the detachment of the composite system at the interface between the UHTSS textile and the mortar and/or at the interface between the mortar and the concrete substrate, with damage of the external face of the concrete cover.

The beam with the single-layered U-wrapped SRG jacket (BUL1, Table 1) failed suddenly when the textile between the mid-point of the shear-critical region and the loading point was detached. The state of the critical region of the beam at the end of the test and after exposing the substrate, is shown in Figs. 9a and 9b, respectively. It is observed that only a single shear crack formed, having the same inclination as that in the original beam B0 (see Fig. 7). In case of the two-layered U-wrapped SRG jacketed beam (BUL2, Table 1), the detachment of the composite system occurred at two stages. First, part of the textile placed between the support and the mid-point of the critical region was detached. The beam continued to carry load and, at a later stage, the textile between the mid-point of the critical span and the loading point was detached. Fig. 9c shows the BUL2 beam at the end of the test. Again, as shown in Fig. 9d, one single crack formed with the same inclination as the crack in the original beam B0 (see Fig. 7).

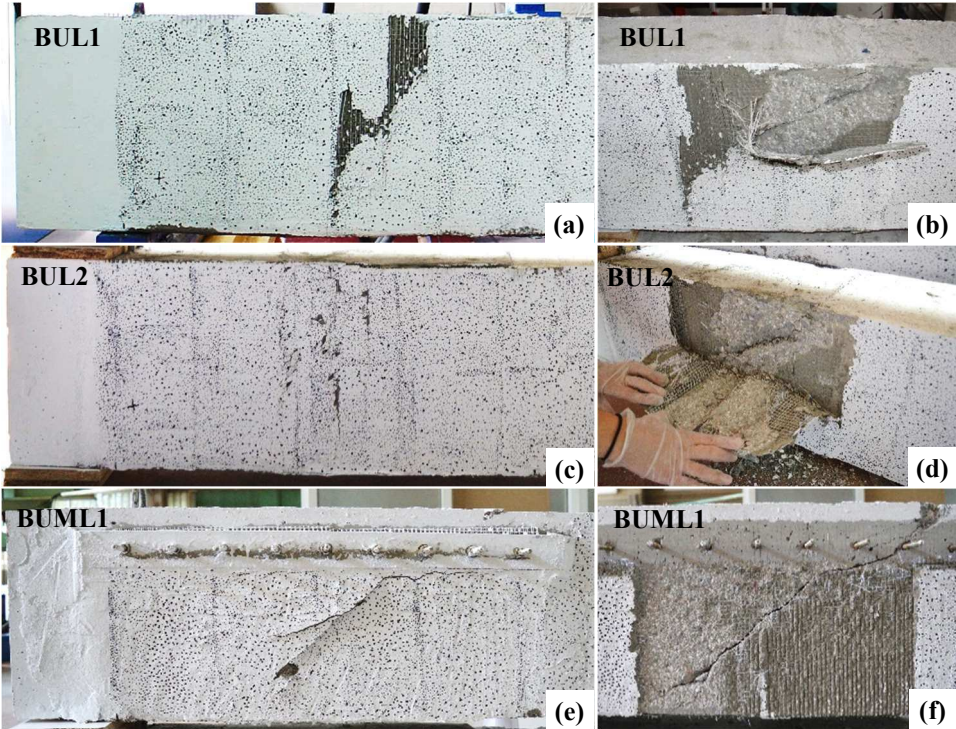


Figure 9: Failure modes of the U-wrapped SRG beams of Group B in the shear-critical span.

After the first stages of loading of the U-wrapped beam with the mechanical anchorage (BUML1, Table 1), an inclined crack formed on the jacket surface below the metal plate, as

shown in Fig. 9e. The existing crack became wider as the load increased. Soon enough the textile detached by forming a new horizontal crack along the bottom side of the metal plate and headed towards the loading point (Fig. 9e). The test was terminated when the inclined crack propagated towards the loading point passed through one of the stud anchors (Fig. 9f). The removal of the jacket and the metal plates revealed that the dominant mode of failure was diagonal tension failure (Fig. 9f) as also observed in the other U-wrapped beams. The SRG jacket remained intact and no damage was visible in the mechanical anchorage system.

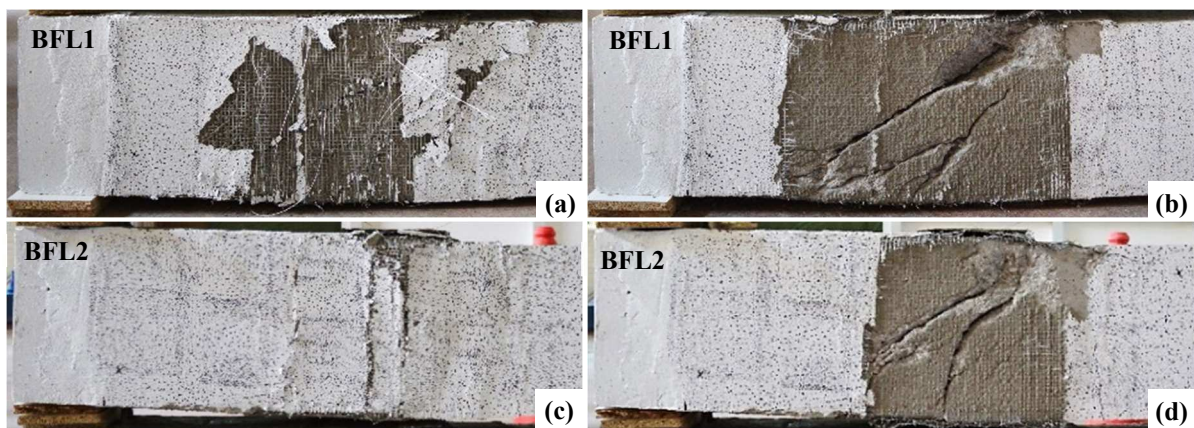


Figure 10: Failure modes of the fully-wrapped SRG beams of Group B in the shear-critical span.

The fully-wrapped SRG beams (BFL1 and BFL2, Table 1) behaved in a more ductile manner compared to the U-wrapped and the original beams. In case of BFL1 beam, a shear-flexure crack formed on the jacket surface within the critical region at the initial stage of loading. As the load increased, damage localized within the inclined area bounded between the loading point and a 150 mm distance from the support, until the external surface of the SRG jacket was heavily cracked (Fig. 10a). At this stage, the beam could not sustain any additional load, but it continued to deform due to passive confinement provided by the SRG jacket. The beam exhibited a ductile behaviour up to the point where gradual rupture of the cords initiated at the upper and bottom sharp edges on both beam faces. The beam failed due to debonding of the textile in the anchorage region (i.e. the region where the end of the fabric overlapped with the

beginning of the textile) next to the applied point load. The cracking pattern of beam BFL1 was different from that of the U-wrapped beams and more flexure-shear cracks were observed as shown in Fig. 10b. Similar to the previous case, beam BFL2 failed in a ductile manner with the internal tensile steel reinforcement reaching yielding. At the initial stage of loading, the first flexural crack appeared in the middle of the SRG jacketed shear span. Subsequently, two more flexural cracks appeared in the opposite side of the critical shear span (i.e. the un-strengthened side of the beam) next to the applied point load. As the load increased, no additional flexural cracks were developed, whereas the existing ones became wider. The confinement provided by two-layered SRG jackets could significantly increase the deflection capacity of the beam, and therefore, the beam managed to sustain the load applied after yielding. The rupture of the cords occurred gradually, and it was mainly concentrated between the mid-point of the shear span and the point at which the load applied. The beam finally failed when the free end-zone of the textile was detached from the anchorage region next to the applied point load. The flexural cracks developed in the critical shear span are shown in Fig. 10d.

The evolution of damage in the SRG jacketed beams of Group B was influenced by the SRG jacket configuration applied, as shown in Fig. 11. Although the U-wrapped SRG jackets could not prevent shear failure, this was delayed until higher levels of loading. It is observed that similar to the control beam (B0), a single inclined crack was appeared in the U-wrapped beams (BUL1, BUL2, BUML1). The response of the SRG jacketed beams was improved substantially when SRG closed-type jackets (i.e. fully-wrapped) were applied. The confinement provided by the one-layered fully-wrapped jacket (BFL1) led to a ductile behaviour upon shear failure with the presence of a multiple shear–flexure cracking pattern (Fig. 11). The two-layered fully-wrapped SRG jacket (BFL2) improved substantially the response of the original beam by alleviating the deficiencies related to old type detailing. The SRG jacketed beam failed in flexure with flexural cracks formed near the applied point load.

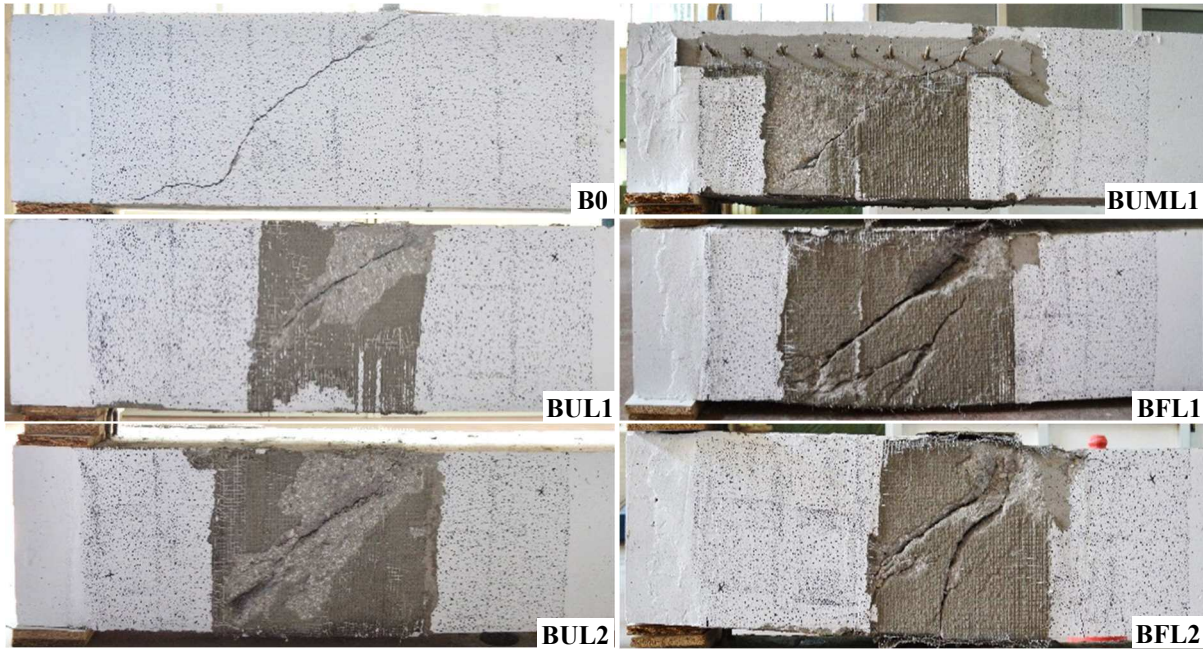


Figure 11: Crack patterns at failure in Group B beams

3.2 Load deflection curves

The load deflection response curves of Group A and B specimens are presented in Fig. 12. A summary of the test results is also provided in Table 4. The key performance parameters include the peak load (P_{max}) and the corresponding deflection (δ_{max}), the ultimate load at a 20 % drop of the peak load (P_u) and the corresponding deflection (δ_u), and finally the displacement ductility (μ_δ). In case that no descending branch appears in the load–deflection curve, the last point of the curve is considered as the ultimate deflection (δ_u). The displacement ductility was defined after idealizing the experimental load–deflection curve by a bilinear curve according to the recommendations of ASCE/SEI Standard 41-06 recommendations [42].

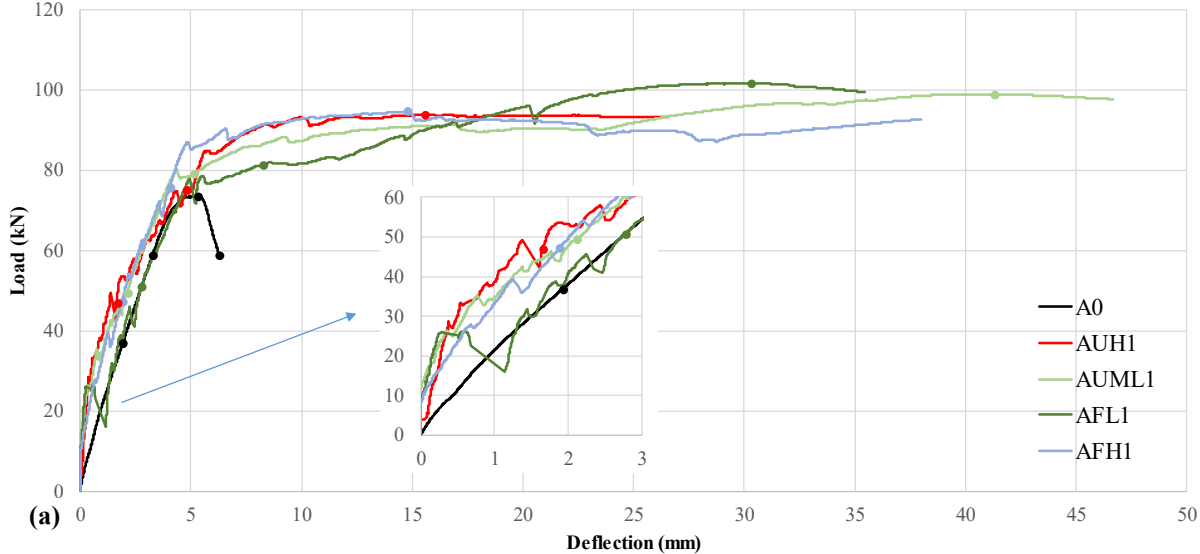
In general, the results indicate that the SRG shear strengthening intervention could considerably improve the strength and deformation capacity of the control beams. The different jacket configurations applied in Group A beams showed the same level of efficiency in modifying the structural response from brittle to ductile (Fig. 12a). The strength increase at peak load varied between 27.6 to 38.1 %, whereas the displacement ductility ranged between 9.1 to 12.3 (Table 4). The lowest increase in the strength and displacement ductility levels was

observed for the high density U- and fully-wrapped SRG jackets (AUH1 and AFH1). This is because when dense textiles are used in SRG applications, as for example the 4.72 cords/cm density textile, the small gaps between the cords impose difficulties in the penetration of the mortar. Hence, the fact that the cords are not well embedded in the mortar renders the SRG system less efficient. A similar observation was reported by Thermou et al. [19] for retrofitting of RC columns using SRG jacketing. The main conclusion drawn from Group A beams is that in case of lightly reinforced RC beams ($\rho_l = 0.75\%$), which are representative of the old construction practice in southern Europe, the lower density (1.57 cords/cm) U-wrapped jackets can be very effective in preventing shear failure and modifying the response from brittle to ductile.

The effect of the type of the SRG jacket on the load–deflection response of Group B beams is shown in Fig. 12b. The control beam (B0) failed by diagonal tension failure at a peak load of 105.6 kN (Table 4). The single- and doubled-layered U-wrapped beams (BUL1, BUL2) as well as the single-layered U-wrapped beam with the mechanical anchorage (BUML1) failed in shear at peak loads of 216.7, 221.1 and 225.7 kN, respectively (Table 4). The increase in the strength of BUL1, BUL2 and BUML1 beams compared to the control beam (B0) at peak load was 105, 110 and 114 %, respectively. The deflection increase at ultimate load was 73, 55 and 77 % for BUL1, BUL2 and BUML1 beams, respectively. As observed, the U-wrapped SRG jacket with the mechanical anchorage (BUML1) exhibited the highest load and deflection increase amongst the U-wrapped jackets. This is mainly attributed to the presence of the mechanical anchorage which kept the jacket in place for a higher sustained load compared to the other two U-wrapped SRG jackets (i.e. BUL1, BUL2) and thus contributed further to the resistance of the beam. It can be noted that the single-layered fully-wrapped SRG jacket (BFL1) reached the same peak load as the single-layered U-wrapped SRG jacket with the mechanical anchorage (BUML1) but presented a more ductile post-peak load-deflection response. The fully-wrapped jacketed beam

deformed up to 20.7 mm deflection at ultimate load, which implies that 349 % increase in the deflection capacity (or deformability) was achieved compared to the control beam before failing due to debonding of the textile in the anchorage region. The displacement ductility for BFL1 beam was estimated equal to 3.4. Using two-layered fully-wrapped SRG jackets in BFL2 beam could substantially increase the shear strength allowing flexural failure to occur. The peak load in this case was 274.2 kN, which corresponds to almost 160 % increase when compared to the control beam (B0). The second layer of full jacket increased the deflection at ultimate to 25.5 mm. The displacement ductility was estimated equal to 3.8, which is rather satisfying considering the inherent deficiency of the beam.

Comparison between the results for BLF1 and BLF2 beams shows that increasing the number of SRG layers had a limited effect (around 10%) on the ductility of the specimens, while it could considerably increase the maximum strength and deflection capacity of the specimens (up to 23%). The results in Table 4 also indicate that SRG jacketing was more efficient in increasing the deformation capacity and ductility of the beams with lower longitudinal reinforcement ratio (i.e. Group A). However, the effect of SRG jacketing on improving the maximum strength was more pronounced for the beam elements with higher longitudinal reinforcement ratio (i.e. Group B).



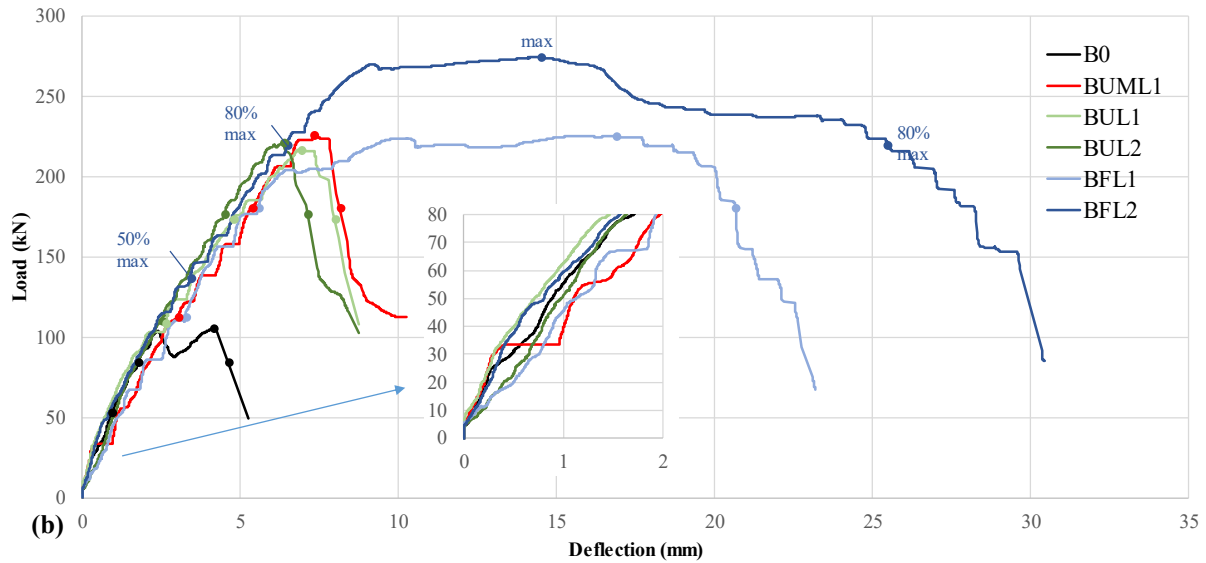


Figure 12: Load-deflection curves for (a) Group A; (b) Group B beams.

Table 4: Summary of test results

Group	Name	P_{max} (kN)	P_u (kN)	δ_{max} (mm)	δ_u (mm)	Strength increase at peak (%)	Deflection increase at ultimate (%)	Ductility μ_δ	Failure mode
Group A	A0	73.6	58.9	5.3	6.2	-	-	-	Shear
	AUH1	93.9	93.0	15.5	26.5	27.6	326.0	9.1	Flexural
	AUML1	98.8	97.6	41.3	46.7	34.3	649.3	12.3	Flexural
	AFL1	101.6	99.4	29.2	34.4	38.1	452.5	12.1	Flexural
	AFH1	94.6	92.6	14.8	38.0	28.5	510.0	10.7	Flexural
Group B	B0	105.6	84.5	4.2	4.6	-	-	-	Shear
	BUL1	216.7	173.3	6.9	8.0	105.2	73.3	-	Shear
	BUL2	221.1	176.9	6.4	7.1	109.5	55.0	-	Shear
	BUML1	225.7	180.5	7.3	8.1	113.8	77.0	-	Shear
	BFL1	225.4	180.4	16.9	20.7	113.5	349.1	3.4	Shear/Flexural
	BFL2	274.2	219.3	14.5	25.5	159.7	453.5	3.8	Flexural

3.3 Evolution of damage based on Digital Image Correlation

As described previously, the additional measurement technique of Digital Image Correlation (DIC) was applied on all specimens by painting a speckle pattern on the shear critical region (area of interest – AOI) of each beam. During testing, a DSLR camera captured high-resolution images of the AOI at given displacement intervals and these images were postprocessed for producing strain contours at preselected characteristic points on the load-displacement response

curve. The characteristic points were selected to represent 50%, 80% and 100% of the peak load (ascending branch) as well as 20% drop of peak load in the descending branch (see Fig. 12). The results were used to demonstrate the evolution of damage on the AOI surface in terms of horizontal (ϵ_x) and vertical (ϵ_y) strain distribution.

Figure 13 shows the strain evolution of the control specimen B0. It is observed that minor flexural cracks started to develop on the bottom edge of the beam up to the attainment of the peak load when the localized diagonal shear crack was formed. At that point, the longitudinal strain (ϵ_x) reached about 1‰, substantially lower than the reinforcement yielding point (about 2.5‰). It is notable that a second shear crack also started to develop parallel to the major one; however, it could not fully form due to the brittle shear failure (no descending branch was captured in this case). It was confirmed that the behaviour of the control beam B0 fully corresponds to the typical textbook shear failure type.

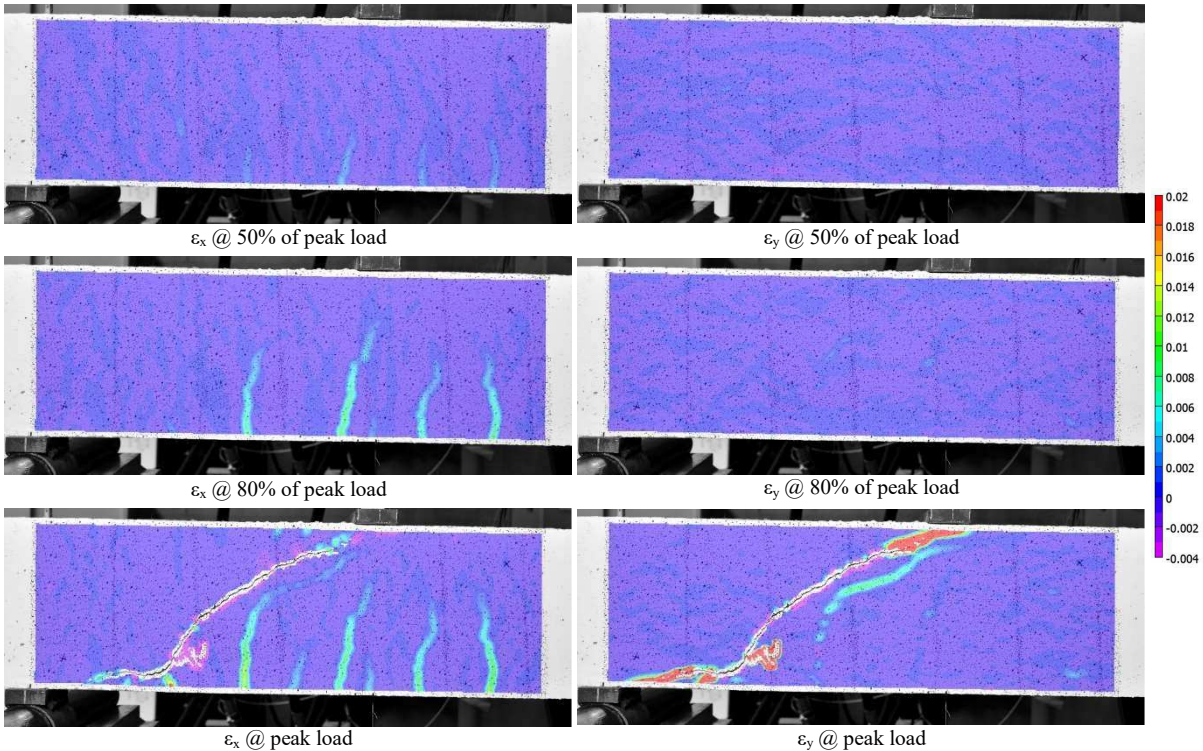


Figure 13: Strain evolution for beam B0 using DIC

The strain evolution of the U-wrapped specimen with single layer (BUL1) is depicted in Fig. 14. In this case, the flexural cracks sustained larger longitudinal strains (well over 2%) at the peak load, where also an inclined yet diffused cracking pattern appeared due to the presence of the SRG U-wrap. This justifies the increased shear strength already recorded during testing for this type of SRG jacketing. For the mechanical anchorage (BUML1) and double-layer U-wrapped (BUL2) specimens, this diffusion was wider, with less inclined straining (i.e. longitudinal strains only) observed, especially for the latter case.

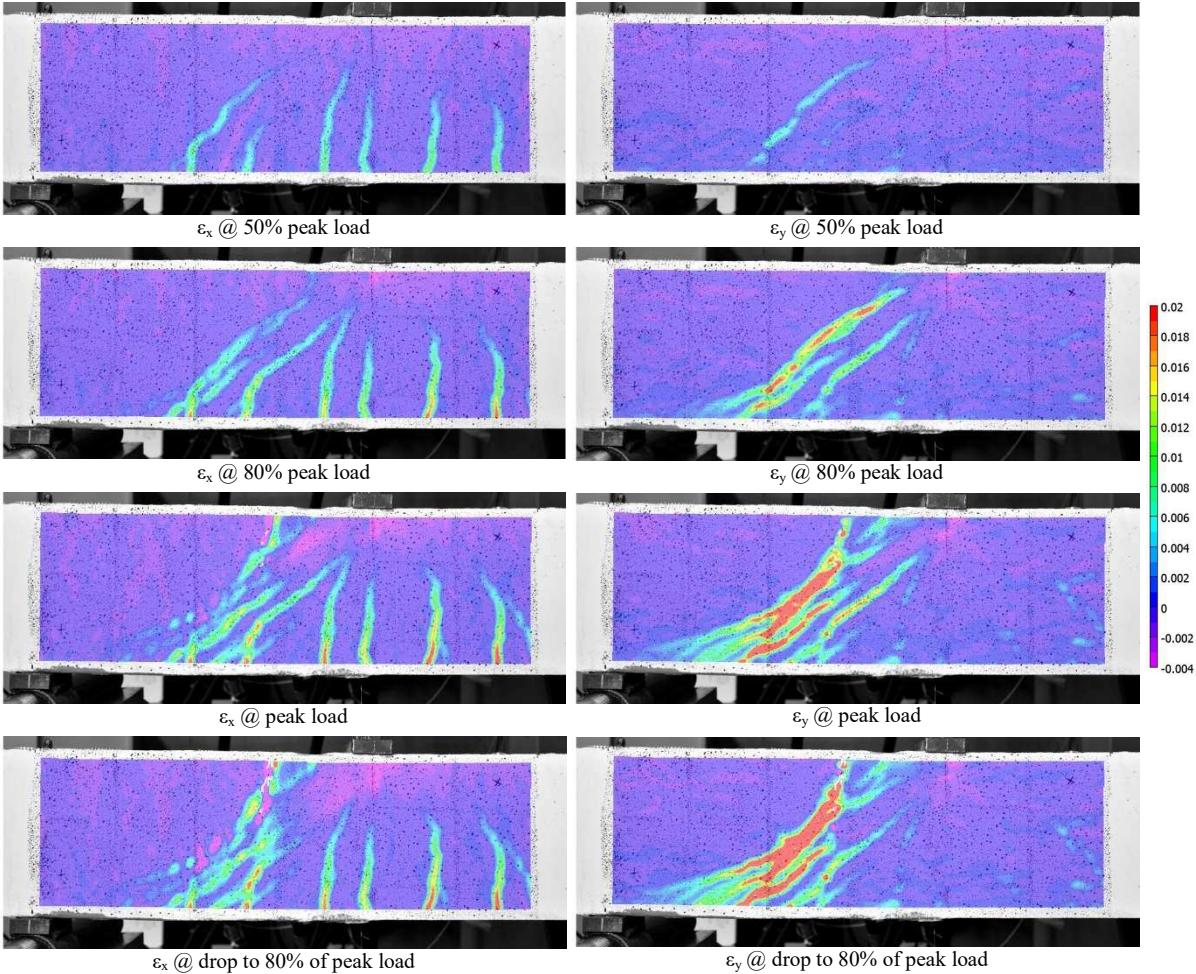


Figure 14: Strain evolution for beam BUL1 using DIC

Finally, for the fully-wrapped cases (BFL1 and BFL2), the strain evolution on the AOI surface shows that the SRG layer(s) completely prevented the development of diagonal straining of the steel material (see Fig 15). It is observed that strains were strongly diffused only

in the longitudinal direction and the failure pattern clearly corresponded to the rupture of the steel cords.

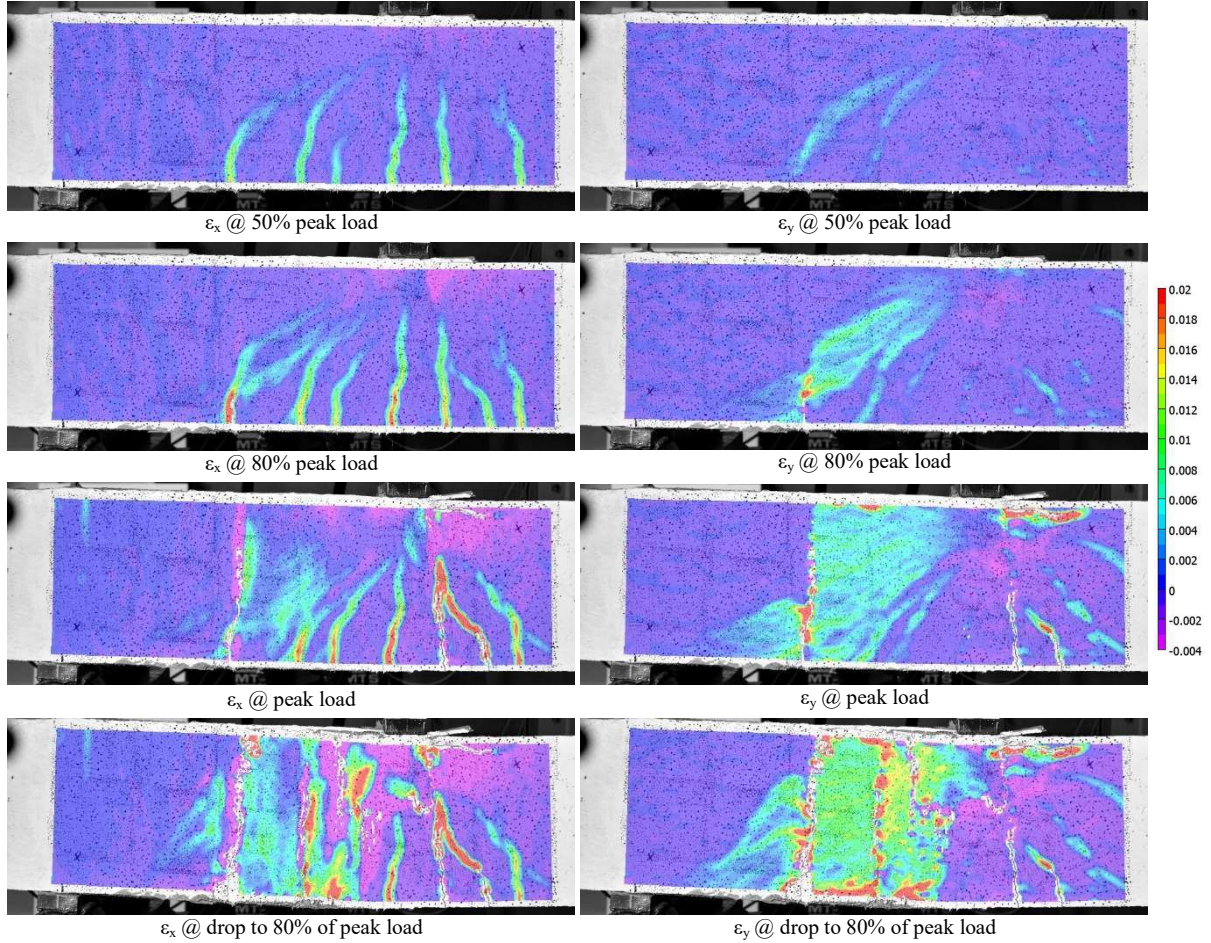


Figure 15: Strain evolution for beam BFL2 using DIC

4. Comparison of experimental results to analytical predictions

4.1 Shear resistance of the SRG jacketed beams

The total shear strength of SRG jacketed RC beams, V_{shear} , comprises shear strength contributions from concrete, (V_c), steel stirrups, (V_s), and SRG jacket, (V_{SRG}):

$$V_{shear} = V_c + V_s + V_{SRG} \leq V_{Rd,max} \quad (1)$$

V_{shear} estimated according to Eq. (1) shall not exceed the limit value for shear, $V_{Rd,max}$, which corresponds to crushing of the diagonal compression struts in the web of the member [43].

Since the studied beams did not contain any stirrups in the critical shear span, the term V_s can

be neglected from Eq. (1). The shear strength contribution from concrete, V_c , is calculated herein by using the EC2 [43] and ACI 318 [44] design guidelines:

$$V_c^{EC2} = 0.12 \cdot k \cdot (100 \cdot \rho_l \cdot f_c)^{1/3} \cdot b_w \cdot d \geq 0.035 \cdot k^{3/2} \cdot f_c^{1/2} \cdot b_w \cdot d \quad (2)$$

$$V_c^{ACI} = 0.167 \sqrt{f_c} \cdot b_w \cdot d \quad (3)$$

where f_c is the concrete compressive strength, b_w is the width of the cross section, d is the depth of the cross section, k ($= 1 + \sqrt{(200/d)} \leq 2$ with d in mm) is a factor that considers the size effect and ρ_l is the area ratio of the tensile reinforcement.

Similar to the approach adopted for other externally bonded composite materials (e.g. FRP, FRCM), the shear strength contribution of the SRG jackets is determined following the truss analogy model [e.g. 45-49]. The steel fabric is considered to have an equivalent thickness per unit width and an effective strain, $\varepsilon_{f,eff}$ [14]. By considering the effects of fibre orientation and assuming a crack pattern, the shear force sustained by the SRG can be calculated as:

$$V_{SRG} = n \cdot \rho_f \cdot b_w \cdot h_f \cdot \varepsilon_{f,eff} \cdot E_f \cdot (\cot \theta + \cot \alpha) \cdot \sin \alpha \quad (4)$$

where n is the number of textile layers applied; ρ_f ($= 2 \cdot t_f / b_w$) is the SRG web reinforcement ratio for a single layer; b_w is the width of the cross section; h_f is the effective depth of the jacket taken as $(h - 0.1d) \approx 0.9d$ (h and d are the height and the effective depth of the cross section, respectively) for full-depth SRG jackets; $\varepsilon_{f,eff}$ is the effective strain in the cords; E_f is the elastic modulus of the SRG fabric; α is the angle between the fibres and the beam axis perpendicular to the shear force; and θ is the angle between the concrete compression strut and the beam axis perpendicular to the shear force.

Depending on whether the textile will be applied in strips of width b_f at a longitudinal distance s_f or as a continuous fabric with an equivalent thickness, t_f , and by considering $\alpha=90^\circ$ (i.e. fibres aligned perpendicular to the horizontal axis) and $\theta=45^\circ$ (i.e. the angle between the

concrete compression strut and the beam axis perpendicular to the shear force), Eq. (4) is simplified to:

$$V_{SRG} = 2 \cdot n \cdot t_f \cdot h_f \cdot \varepsilon_{f,eff} \cdot E_f \quad \text{for continuous fabric} \quad (5a)$$

$$V_{SRG} = 2 \cdot n \cdot t_f \cdot h_f \cdot \frac{b_f}{s_f} \cdot \varepsilon_{f,eff} \cdot E_f \quad \text{for strips} \quad (5b)$$

In Eqs. (4, 5), the effective strain, $\varepsilon_{f,eff}$, corresponds to a fraction of the rupture strain for the cords, ε_{fu} , and is used to account for the non-uniform distribution of stress in the textile intersecting the shear crack and for the reduction of SRG strength due to bending of the fibres at the corners of the cross section. The strain efficiency factor $k_\varepsilon (= \varepsilon_{f,eff} / \varepsilon_{fu} < 1)$ is implemented for estimating the effective strain, $\varepsilon_{f,eff}$.

Different values for k_ε have been suggested by various researchers and code provisions. Based on an experimental study on carbon TRM jackets, Triantafillou and Papanikolaou [24] concluded that $\varepsilon_{f,eff}$ corresponds to approximately 50% of the ultimate strain, ε_{fu} , of the cords. In a different study, by investigating experimentally the performance of RC beams shear strengthened with various TRM jacketing systems, Escrig et al. [34] proposed a methodology for estimating TRM contribution to the shear capacity based on the following expressions for the effective strain, $\varepsilon_{f,eff}$:

$$\varepsilon_{f,eff} = 0.035 \cdot \left(\frac{f_c^{2/3}}{n \cdot E_f \cdot \rho_f} \right)^{0.65} \cdot \varepsilon_{fu} \quad \text{fully wrapped} \quad (6a)$$

$$\varepsilon_{f,eff} = 0.020 \cdot \left(\frac{f_c^{2/3}}{n \cdot E_f \cdot \rho_f} \right)^{0.55} \cdot \varepsilon_{fu} \quad \text{side bonded or U-wrapped} \quad (6b)$$

where f_c (in MPa) is the concrete compressive strength, ε_{fu} is the strain at failure, E_f (in GPa) is the elastic modulus of the textile, and ρ_f is the web reinforcement ratio for a single SRG layer.

The definition of the modulus of elasticity and the effective strain adopted by the ACI 549-9R-13 [46] for the design of externally bonded FRCM systems are based on the behaviour of

the cracked composite material. For the case of effective strain of the SRG composite, $\varepsilon_{f,eff}^*$, an upper limit of 0.004 is used in this study [46]. The modulus of elasticity of the SRG composite, E_f^* , is taken equal to 168000 MPa which corresponds to the average modulus of elasticity defined by tensile tests of the SRG composite [51].

In the following section, the adequacy of the above effective strain definitions (suggested by [24, 34, 46]) to predict the shear capacity of RC beams strengthen by SRG jackets is investigated compared to the experimental results.

4.2 Experimental results versus analytical predictions

The experimental shear strength values corresponding to the shear critical region, V_{shear}^{exp} ($= P_{max} \cdot L_2/L$); where $L_2(=1.1 \text{ m})$ is the longer span and $L(=1.8 \text{ m})$ is the distance between the supports, are presented in Table 5 for all tested specimens (column (3)). The shear strength contributions from concrete, V_c (Eqs. (2) and (3)), and SRG jacket, V_{SRG} (Eq. 5a), are also given in Table 5 (Columns (7)-(11)). V_{SRG} and consequently V_{shear} are calculated by adopting the three alternative definitions for effective strain, $\varepsilon_{f,eff}$, as discussed in the previous section. The experimental values of the shear strength of the SRG jackets, V_{SRG}^{exp} , are provided by subtracting the shear strength of the control specimen, V_c^{exp} , from the shear strength of the SRG jacketed beams, V_{shear}^{exp} (see column (4) in Table 5). The experimental values of the effective strain, $\varepsilon_{f,eff}^{exp}$, are calculated according to column (6) in Table 5:

$$\varepsilon_{f,eff}^{exp} = \frac{V_{shear}^{exp} - V_c^{exp}}{2 \cdot n \cdot t_f \cdot h_f \cdot \varepsilon_{f,eff} \cdot E_f} \quad (7)$$

where n is the number of textile layers applied; t_f is the equivalent thickness of the textile; h_f is the effective depth of the jacket; $\varepsilon_{f,eff}$ is the effective strain; E_f is the elastic modulus of the

textile; and V_{SRG}^{exp} and V_c^{exp} correspond to the experimental values of the shear strength of the SRG jackets and the control specimen, respectively. The same expression can be used for calculating the effective strain of the SRG composite, $\varepsilon_{f,eff}^*$, if the modulus of elasticity of the SRG composite, E_f^* , is used (column (5) in Table 5).

The experimental and the predicted normalized shear stress provided by the SRG system are calculated from:

$$v_{SRG}^{exp} = \frac{V_{SRG}^{exp}}{b_w \cdot d \cdot f_c} \quad (8a)$$

$$v_{SRG} = \frac{V_{SRG}}{b_w \cdot d \cdot f_c} \quad (8b)$$

where b_w is the width of the cross section, d is the depth of the cross section, f_c is the concrete compressive strength, V_{SRG}^{exp} and V_{SRG} correspond to the experimental and analytical values of the shear strength of the SRG jackets, respectively.

Fig. 16 compares the experimental values of the normalized shear stress, v_{SRG}^{exp} , with the predicted ones, v_{SRG} , for the three different definitions of the effective strain, $\varepsilon_{f,eff}$, adopted herein. Based on the observed mode of failure, the beam test data are divided into three categories; no damage to the textile for beams in Group A, debonding of the textile for the U-wrapped Group B beams, and rupture of the textile for the fully-wrapped beams of Group B. The 45° linear lines in Fig. 13 can provide direct insight on whether the adopted model underestimates or overestimates the predicted values for the shear stress, v_{SRG} ; and therefore, determine how safe is to use these particular models. In case of Group A beams, where no damage was observed in the textile, v_{SRG} is overestimated for all the three definitions of the effective strain adopted in this study (see Fig. 13a-c). The ACI 549-9R-13 [46] and Escrig et al.

[34] models generally provided safe results, since the predicted values were lower than the experimental ones for the beams that failed due to debonding and rupture of the textile (see the points plotted above the linear line in Figs. 13a and 13c). For the same modes of failure, the Triantafillou and Papanikolaou [24] model provided both safe and unsafe predictions as illustrated in Fig. 13(b).

The accuracy of the adopted models is further investigated by employing statistical indices such as the mean value (AVR), the standard deviation (STD), the coefficient of variation (COV=STD/AVR) and also the average absolute error (AAE) defined as follows:

$$AAE = \frac{\sum_{i=1}^N \left| \frac{(v_{SRG})_i - (v_{SRG}^{\text{exp}})_i}{(v_{SRG}^{\text{exp}})_i} \right|}{N} \quad (9)$$

where $(v_{SRG})_i$ and $(v_{SRG}^{\text{exp}})_i$ represent the predicted and experimental values of the shear strength and N corresponds to the total number of beams. Table 6 presents the calculated statistical indices for each model based on the mode of failure observed. The minimum AAE value is observed for the Triantafillou and Papanikolaou [24] model when rupture and debonding are the anticipated modes of failure. For the same modes of failure, the minimum COV corresponds to the Escrig et al. [34] model.

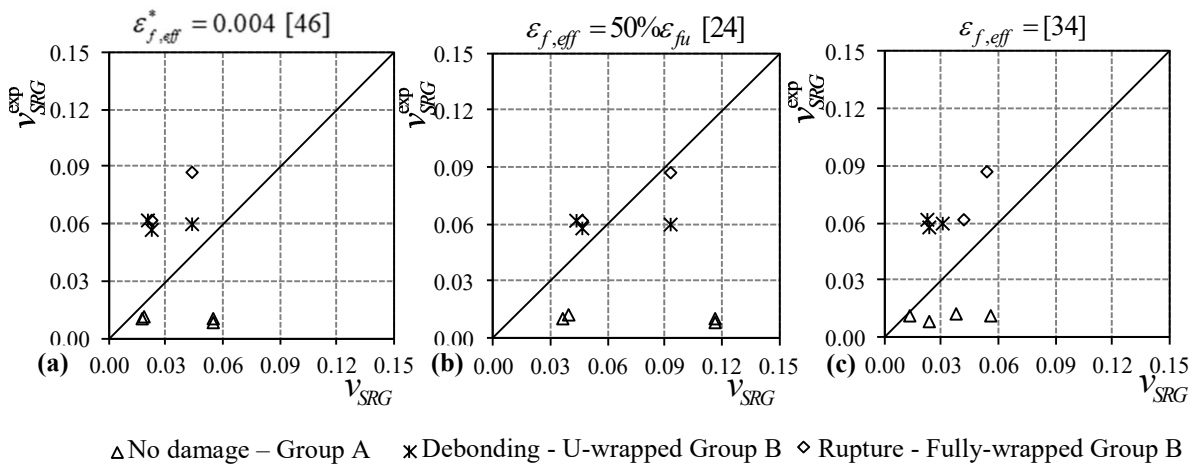


Figure 16: Comparison between experimental, v_{SRG}^{exp} , and predicted, v_{SRG} , shear strength.

1

Table 5: Comparison between experimental and predicted values of shear strength

Group	Specimen	Experimental values					Analytical predictions								
		V_c^{exp} (kN)	V_{shear}^{exp} (kN)	V_{SRG}^{exp} (kN)	$\varepsilon_{f,eff}^{*exp}$ $\times 10^3$	$\varepsilon_{f,eff}^{exp}$ $\times 10^3$	V_c^{ACI} (kN)	V_c^{EC2} (kN)	$\varepsilon_{f,eff}^*$ [46]	$\varepsilon_{f,eff}$ [24]	$\varepsilon_{f,eff}$ [34]	$\varepsilon_{f,eff}^*$ [46]	$\varepsilon_{f,eff}$ [24]	$\varepsilon_{f,eff}$ [34]	
									V_{SRG} (kN)	V_{SRG} (kN)	V_{SRG} (kN)	V_{shear} (kN)	V_{shear} (kN)	V_{shear} (kN)	
	(1)	(2)	(3)	(4)=(3)-(2)	(5)	(6)	(7)	(8)	(9)	(10)	(11)	(12)=(7)+(9)	(13)=(8)+(10)	(14)=(8)+(11)	
A	AUH1	47.6	60.8	13.1	0.63	0.56	47.9	27.4	83.3	176.7	35.8	131.2	204.1	63.2	
	AUML	47.6	63.9	16.3	2.55	2.25	47.9	27.4	25.6	54.3	20.1	73.5	81.8	47.6	
	AFL1	47.6	65.8	18.1	2.61	2.31	47.9	27.4	27.8	58.9	57.3	75.7	86.3	84.7	
	AFH1	47.6	63.9	16.3	0.78	0.69	47.9	27.4	83.3	176.7	84.1	131.2	204.1	111.6	
B	BUL1	68.3	146.0	71.9	10.43	9.22	43.4	39.3	27.6	58.5	30.0	70.9	97.7	69.3	
	BUL2	68.3	140.2	74.8	5.42	4.80	43.4	39.3	55.1	116.9	38.2	98.5	156.2	77.5	
	BUML	68.3	143.1	77.6	12.11	10.71	43.4	39.3	25.6	54.3	27.9	69.0	93.6	67.1	
	BFL1	68.3	145.9	77.6	11.25	9.95	43.4	39.3	27.6	58.5	52.5	70.9	97.7	91.8	
	BFL2	68.3	177.4	109.1	7.92	7.00	43.4	39.3	55.1	116.9	66.9	98.5	156.2	106.2	

2

3

4

5

6

7

Table 6: Statistical indices for v_{SRG}^{exp}/v_{SRG}

Statistical indices	No damage			Debonding			Rupture		
	$\epsilon_{f,eff}^*$	$\epsilon_{f,eff}$	$\epsilon_{f,eff}$	$\epsilon_{f,eff}^*$	$\epsilon_{f,eff}$	$\epsilon_{f,eff}$	$\epsilon_{f,eff}^*$	$\epsilon_{f,eff}$	$\epsilon_{f,eff}$
	[46]	[24]	[34]	[46]	[24]	[34]	[46]	[24]	[34]
AVR	3.64	7.72	3.07	0.48	1.03	0.43	0.43	0.91	0.64
STD	2.46	5.23	1.62	0.22	0.47	0.08	0.11	0.22	0.04
COV	67.7%	67.7%	52.7%	45.7%	45.7%	17.9%	24.6%	24.6%	7.0%
AAE	263.9%	671.7%	206.8%	51.6%	35.0%	57.1%	57.0%	15.9%	35.5%

For better comparison, the normalized experimental value of the effective strain, $\epsilon_{f,eff}^{exp}/\epsilon_{fu}$, is plotted against the quantity $\rho_f \cdot E_f/f_c^{2/3}$ in Fig. 17. The term $\rho_f \cdot E_f$ expresses the axial rigidity of the textile or the composite in case the modulus of elasticity is that of the composite, E_f^* . The term $f_c^{2/3}$ is related to the tensile strength of the concrete, where f_c is the compressive strength of concrete. It is shown in Fig. 17 that, similar to observations made for FRP composites [52], $\epsilon_{f,eff}^{exp}/\epsilon_{fu}$ decreases as $\rho_f \cdot E_f/f_c^{2/3}$ increases. The horizontal line corresponds to $\epsilon_{f,eff}^{exp}/\epsilon_{fu} = 50\%$ [24].

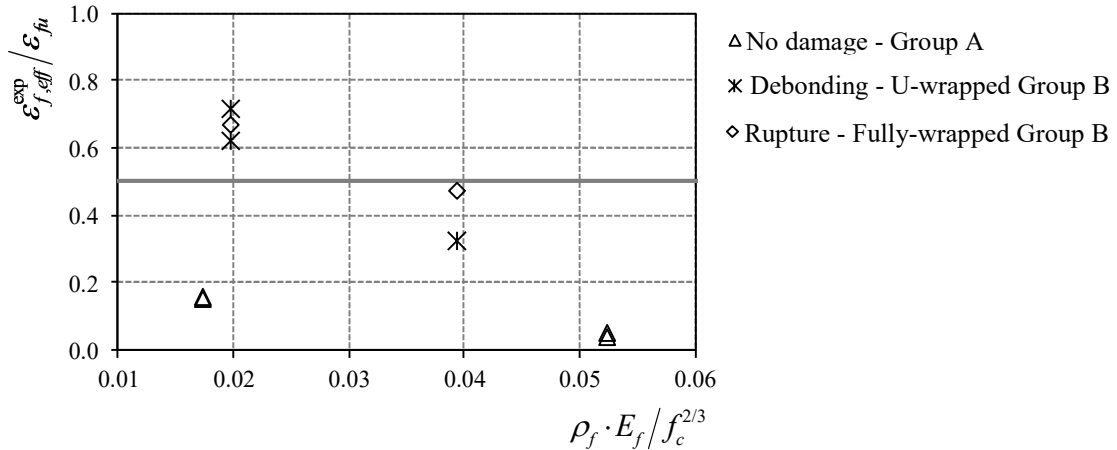


Figure 17: Normalized experimental effective strain, $\epsilon_{f,eff}^{exp}/\epsilon_{fu}$, versus $\rho_f \cdot E_f/f_c^{2/3}$.

The experimental data were used to derive best fit curves that relate $\epsilon_{f,eff}^{exp}/\epsilon_{fu}$ to $\rho_f \cdot E_f/f_c^{2/3}$ as presented in Fig. 18. It should be mentioned that the U-wrapped beams with the mechanical

anchorage (AUML1 and BUML1 in Table 1) were excluded from the utilized data since the objective was to include only specimens where no additional connection measures for the jackets were taken. The following expressions have been derived:

$$\varepsilon_{f,eff} = 0.010 \cdot \left(\frac{f_c^{2/3}}{n \cdot E_f \cdot \rho_f} \right)^{0.47} \cdot \varepsilon_{fu} \quad \text{no damage in the textile} \quad (10a)$$

$$\varepsilon_{f,eff} = 0.015 \cdot \left(\frac{f_c^{2/3}}{n \cdot E_f \cdot \rho_f} \right)^{0.94} \cdot \varepsilon_{fu} \quad \text{side bonded or U-wrapped} \quad (10b)$$

$$\varepsilon_{f,eff} = 0.066 \cdot \left(\frac{f_c^{2/3}}{n \cdot E_f \cdot \rho_f} \right)^{0.59} \cdot \varepsilon_{fu} \quad \text{fully wrapped} \quad (10c)$$

It should be noted that the above equations are based on limited experimental data and need to be verified by more data before used for practical design purposes. However, the results of this study should prove useful in understanding the influence of key design parameters on the effectiveness of shear strengthening of RC beams using SRG jackets.

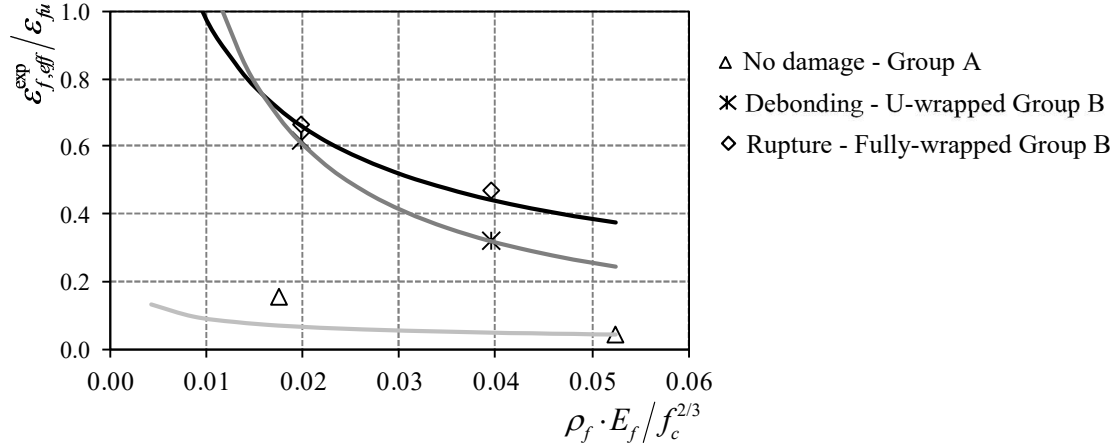


Figure 18: Best fit curves that relate $\varepsilon_{f,eff}^{exp} / \varepsilon_{fu}$ to $\rho_f \cdot E_f / f_c^{2/3}$.

5. CONCLUSIONS

An experimental study was carried out to investigate the effectiveness of SRG jacketing as a relatively new composite system for strengthening shear-deficient RC beams. Eleven two-span RC beams were constructed and classified into two groups according to the arrangement of the internal reinforcement. Two of the beams served as control specimens whereas the rest were strengthened with one- or two-layered U-wrapped, U-wrapped with mechanical anchorage and fully-wrapped SRG jackets. Apart from the jacket configuration, parameters of study were the density of the fabric and the number of layers. Digital Image Correlation (DIC) was applied on all specimens to produce strain contours at several characteristic points on the load-displacement response curve. The strain evolution within the critical span and the crack patterns were analysed, while the rupture of the steel cords was verified by the strains diffusion observed in the longitudinal direction. The main conclusions drawn from this study are summarized as follows:

- The different types of SRG jackets applied to the lightly-reinforced Group A beams ($\rho_l = 0.75\%$) could increase the peak load capacity and displacement ductility by up to 38% and 12%, respectively. In all cases the shear failure was prevented, and the response was modified from brittle to ductile.
- The U-wrapped SRG beams of Group B ($\rho_l = 1.60\%$) failed in shear due to detachment of the composite system in the shear-critical region. The use of the suggested mechanical anchorage system could keep the SRG jacket in place for a higher sustained load compared to the U-wrapped SRG beams. The average strength and deflection capacity increase of the U-wrapped beams compared to the control beam was 110% and 70%, respectively.
- The single-layered fully-wrapped SRG jacket applied on Group B beams resulted in a ductile behaviour (displacement ductility $\mu_s = 3.4$) upon failure with the presence of multiple shear–flexure cracks. The two-layered fully-wrapped SRG jacket modified substantially the

response of the original member by allowing it to fail in flexure (displacement ductility $\mu_s = 3.8$). The maximum strength increased to 114 and 160% of that of the original shear deficient beam by using single-layered and two-layered fully-wrapped SRG jackets, respectively.

- The experimental values of the shear stress were compared to the predicted ones utilizing the effective strain as defined by Triantafillou and Papanicolaou [24], Escrig et al. [34] and ACI 549-9R-13 [44]. The minimum AAE value was observed for the Triantafillou and Papanicolaou [24] model when rupture and debonding are the anticipated modes of failure.
- Based on the experimental data of current study, new expressions were developed for estimating the effective strain of the SRG jacket using different jacketing systems as a function of the axial rigidity of the SRG textile. However, more experimental data are required to assess the validity of the proposed expressions before they can be widely adopted.

The results of this study in general indicate that the SRG jacketing can be considered as a promising strengthening technique for shear-deficient RC beams. Further investigation is deemed necessary on the interaction of internal and externally bonded SRG reinforcement.

ACKNOWLEDGMENTS

The experimental program was conducted in the Laboratory of Reinforced Concrete and Masonry Structures, Civil Engineering Department, Aristotle University of Thessaloniki. Special thanks are attributed to Interbeton and Kerakoll S.p.A. for providing the materials. This project has received funding from the European Union's Horizon 2020 research and innovation programme under the Marie Skłodowska-Curie grant agreement No. 700863.

REFERENCES

- [1]. G.E. Thermou, S.J. Pantazopoulou, Assessment indices for the seismic vulnerability of existing RC buildings. *Journal of Earthquake Engineering and Structural Dynamics*, (2011) 40 (3), 293-313.
- [2]. S.J. Pardalopoulos, G.E. Thermou, S.J. Pantazopoulou, Screening Criteria to Identify Brittle RC Structural Failures in Earthquakes. *Bulletin of Earthquake Engineering*, (2013), 11(2), 607–636.
- [3]. G.E. Thermou, M. Psaltakis, Retrofit design methodology for substandard R.C. buildings with torsional sensitivity. *Journal of Earthquake Engineering* (2018). DOI: 10.1080/13632469.2016.1277569.
- [4]. H. Saadatmanesh, M.R. Ehsani, L. Jin, Repair of earthquake - damaged RC columns with FRP wraps. *ACI Struct. J.* 94(2) (1997) 206-215.
- [5]. F. Seible, M.J.N. Priestley, G.A. Hegemier, Seismic retrofit of RC columns with continuous carbon fiber jackets. *ASCE J. of Comp. for Constr.* 1(2) (1997) 52-62.
- [6]. K.A. Harries, J.R. Ricles, S. Pessiki, R. Sause, Seismic retrofit of lap-splices in non-ductile square columns using carbon fiber-reinforced jackets. *ACI Struct. J.* 103(6) (2006) 874-884.
- [7]. G.E. Thermou, S.J. Pantazopoulou, Fiber reinforced polymer retrofitting of substandard RC prismatic members. *Journal of Composites for Construction*. ASCE 13(6) (2009) 535-546.
- [8]. T.C. Triantafillou, C.G. Papanicolaou, P. Zissimopoulos, T. Laourdekis, Concrete confinement with textile-reinforced mortar jackets. *ACI Struct. J.* 103(1) (2006) 28–37.
- [9]. T.C. Triantafillou, C.G. Papanicolaou, Shear strengthening of reinforced concrete members with textile reinforced mortar (TRM) jackets. *Mater Struct* 39(285) (2006) 93-103.

- [10]. D.A. Bournas, P.V. Lontou, C.G. Papanicolaou, T.C. Triantafillou, Textile-reinforced mortar versus fiber-reinforced polymer confinement in reinforced concrete specimens. *ACI Struct J* 104(6) (2007) 740-748.
- [11]. A. D'Ambrisi, L.Feo, F. Focacci, Experimental analysis on bond between PBO-FRCM strengthening materials and concrete. *J Compos B Eng* 44(1) (2013) 524-532.
- [12]. A. D'Ambrisi, L. Feo, F. Focacci, Bond-slip relations for PBO-FRCM materials externally bonded to concrete. *J Compos B Eng* 43(8) (2012) 2938-2949.
- [13]. G.E. Thermou, S.J. Pantazopoulou, Metallic fabric jackets: an innovative method for seismic retrofitting of substandard RC prismatic members. *fib Struct. Concr. J.* 8(1) (2007) 35-46.
- [14]. G.E. Thermou, K. Katakalos, G. Manos, Concrete confinement with steel-reinforced grout jackets. *Mater. Struct.* 48(5) (2015) 1355-1376.
- [15]. G.E. Thermou, K. Katakalos, G. Manos, Influence of the cross section shape on the behaviour of SRG-confined prismatic concrete specimens. *Mater. Struct.* 49(3) (2016) 869-887.
- [16]. G.E. Thermou, K. Katakalos, G. Manos, Influence of the loading rate on the axial compressive behavior of concrete specimens confined with SRG jackets. *ECCOMAS Thematic Conference COMPDYN, Greece, Kos, Paper No. 1482, 2013.*
- [17]. G.E. Thermou, I. Hajirasouliha, Compressive behaviour of concrete columns confined with Steel-Reinforced Grout jackets. *Comp. Part B: Eng.* 138 (2018) 222-231.
- [18]. G.E. Thermou, I. Hajirasouliha, Design-oriented models for concrete columns confined by steel-reinforced grout jackets. *Construction and Building Materials*, 178 (2018) 313-326.

- [19]. G.E. Thermou, K. Katakalos, G. Manos, Experimental investigation of substandard RC columns confined with SRG jackets under compression. *Composite Structures*, 184 (2018) 55-65.
- [20]. G.E. Thermou, G. de Felice, S. De Santis, S. Alotaibi, F. Roscini, I. Hajirasouliha, M. Guadagnini, Mechanical characterization of multi-ply steel reinforced grout composites for the strengthening of concrete structures. 9th International Conference on Fibre-Reinforced Polymer (FRP) Composites in Civil Engineering (CICE 2018), Paris 17-19, (2018) Paper No. 30.
- [21]. G.E. Thermou, I. Hajirasouliha, Assessment of compressive strength of steel-reinforced grout jacketed concrete columns. 9th International Conference on Fibre-Reinforced Polymer (FRP) Composites in Civil Engineering (CICE 2018), Paris 17-19, (2018), Paper No. 69.
- [22]. G.E. Thermou, I. Hajirasouliha, Evaluating the confining effects of steel-reinforced grout jacketing: An experimental study. ACIC 2017, Sheffield, UK, (2017) Paper No. 56.
- [23]. G.E. Thermou, V.K. Papanikolaou, I. Hajirasouliha, A Novel method for seismic retrofitting of substandard RC columns using steel-reinforced grout jacketing. 16th European Conference on Earthquake engineering, Thessaloniki, Greece, (2018) Paper No. 11063.
- [24]. T.C. Triantafillou, C.G. Papanicolaou, Shear strengthening of reinforced concrete members with textile reinforced mortar (TRM) jackets. *Materials and Structures* (2006) 39:93–103
- [25]. Y. Al-Salloum, M. Elsanadedy, S. Alsayed, R. Iqbal, Experimental and numerical study for the shear strengthening of reinforced concrete beams using textile reinforced mortar, *J. Compos. Construct.* 16(1) (2012) 74–90.

- [26]. R. Azam, K. Soudki, FRCM Strengthening of Shear-Critical RC Beams. *Journal of Composites for Construction*, 04014012, (2014).
- [27]. D. Baggio, K. Soudki, M., Noel Strengthening of shear critical RC beams with various FRP systems. *Constr Build Mater* 66 (2014) 634-44.
- [28]. Z.C. Tetta, L.N. Koutas, D.A. Bournas, Textile-reinforced mortar (TRM) versus fiber-reinforced polymers (FRP) in shear strengthening of concrete beams. *Composites Part B* 77 (2015) 338-348.
- [29]. S.M. Raoof, D.A. Bournas, TRM versus FRP in flexural strengthening of RC beams: Behaviour at high temperatures. *Construction and Building Materials* 154 (2017) 424–437.
- [30]. R. Azam, K. Soudki, J.S. West, M. Noël, Strengthening of shear-critical RC beams: Alternatives to externally bonded CFRP sheets. *Construction and Building Materials* 151 (2017) 494–503.
- [31]. J.H. Gonzalez-Libreros, C. Sabau, L.H. Sneed, C. Pellegrino, G. Sas, State of research on shear strengthening of RC beams with FRCM composites. *Construction and Building Materials* 149 (2017) 444–458.
- [32]. A. Younis, U. Ebead, K.C. Shrestha. Different FRCM systems for shear-strengthening of reinforced concrete Beams. *Construction and Building Materials* 153 (2017) 514–526.
- [33]. T. Trapko, D.a Urbańska, M. Kamiński, Shear strengthening of reinforced concrete beams with PBO-FRCM composites. *Composites Part B* 80 (2015) 63-72.
- [34]. C. Escrig, L. Gil, E. Bernat-Maso, F. Puigvert, Experimental and analytical study of reinforced concrete beams shear strengthened with different types of textile-reinforced mortar. *Construction and Building Materials* 83 (2015) 248–260.
- [35]. Ombers L. (2015) Structural performances of reinforced concrete beams strengthened in shear with a cement based fiber composite material. *Compos Struct* 122 (2015) 316-329.

- [36]. G. Loreto, S. Babaeidarabad, L. Leardini, A. Nanni, RC beams shear-strengthened with fabric-reinforced cementitious- matrix (FRCM) composite. *Int J Adv Struct Eng* 7 (2015) 341–352.
- [37]. Z.R. Aljazaeri, J.J. Myers, Strengthening of Reinforced-Concrete Beams in Shear with a Fabric-Reinforced Cementitious Matrix. *J. Compos. Constr.* 21(5) (2017) 04017041.
- [38]. J.H. Gonzalez-Libreros, L.H. Sneed, T. D’Antino, C. Pellegrino, Behavior of RC beams strengthened in shear with FRP and FRCM composites. *Engineering Structures* 150 (2017) 830–842.
- [39]. A. Napoli, G. de Felice, S. De Santis, R. Realfonzo, Bond behaviour of Steel Reinforced Polymer strengthening systems. *Composite Structures* 152 (2016) 499–515.
- [40]. S. De Santis, A. Napoli, G. de Felice, R. Realfonzo, Strengthening of structures with Steel Reinforced Polymers: A state-of-the-art review. *Compos Part B-Eng* 104 (2016): 87-110.
- [41]. Dutton, W.A. Andy, N.A. Hoult, Curvature monitoring of beams using Digital Image Correlation. *J. Bridge Eng., ASCE*, 19(3) (2014) 05013001-13.
- [42]. ASCE 41-06. Seismic rehabilitation of existing buildings. Edition: 1st. American Society of Civil Engineers; 2007
- [43]. Eurocode 2. Design of concrete structures—Part 1-1: General rules and rules for buildings. prEN 1992-1-1:2003E, European Committee for Standardization (CEN), Brussels, 2003.
- [44]. ACI 318-08. Building code requirements for reinforced concrete and commentary. American Concrete Institute, Farmington Hills, MI, 467.
- [45]. American Concrete Institute (ACI) Committee, Guide for the design and construction of externally bonded FRP systems for strengthening concrete structures, ACI 440.2R-08, Farmington Hills, MI, 2008.

- [46]. ACI (American Concrete Institute), Guide to design and construction of externally bonded fabric-reinforced cementitious matrix systems for repair and strengthening concrete and masonry structures, ACI 549.4 R-13, ACI Committee 549, Farmington, MI, 2013.
- [47]. fib Bulletin 14, Externally bonded FRP reinforcement for RC structures, Report by Task group 9.3, fédération internationale du béton (fib), Lausanne, Switzerland, 2001
- [48]. A. Khalifa, W.J. Gold, A. Nanni, A.M.I. Aziz, Contribution of externally bonded FRP to shear capacity of RC flexural members. *ASCE Journal of Composites for Construction*, 2(4) (1998) 195-202.
- [49]. T.C. Triantafillou Shear strengthening of reinforced concrete beams using epoxy-bonded FRP composites. *ACI Structural Journal* 95(2) (1998) 107-115.
- [50]. S.J. Pantazopoulou, S.P. Tastani, G.E. Thermou, T. Triantafillou, G. Monti, D. Bournas, M. Guadagnini, Background to European seismic design provisions for the retrofit of R.C. elements using FRP materials. *Structural Concrete, Journal of the fib*, 17(2) (2016) 133–305.
- [51]. S. De Santis, G. de Felice, Steel reinforced grout systems for the strengthening of masonry Structures. *Composite Structures* 134 (2015) 533–548.
- [52]. C.P. Antonopoulos, T.C. Triantafillou, Experimental investigation of FRP-strengthened RC beam-column joints. *Journal of Composites for Construction* 7(1) (2003) 39-49.